Unpolarized gluon PDF of the nucleon from lattice QCD in the continuum limit



Chen Chen, 1,2 Hongxin Dong, 1,3 Liuming Liu, 1,2,* Peng Sun, 1,2,† Xiaonu Xiong, 4
Yi-Bo Yang, 5,6,7,8,‡ Fei Yao, 9 Jian-Hui Zhang, 10,§ Chunhua Zeng, 1,2 and Shiyi Zhong 10

1 Institute of Modern Physics, Chinese Academy of Sciences, Lanzhou 730000, China

2 University of Chinese Academy of Sciences, School of Nuclear Science and Technology, Beijing 100049, China

3 Nanjing Normal University, Nanjing, Jiangsu 210023, China

4 School of Physics and Electronics, Central South University, Changsha 418003, China

5 University of Chinese Academy of Sciences, School of Physical Sciences, Beijing 100049, China

6 CAS Key Laboratory of Theoretical Physics, Institute of Theoretical Physics,

Chinese Academy of Sciences, Beijing 100190, China

7 School of Fundamental Physics and Mathematical Sciences,

Hangzhou Institute for Advanced Study, UCAS, Hangzhou 310024, China

8 International Centre for Theoretical Physics Asia-Pacific, Beijing/Hangzhou, China

9 Physics Department, Brookhaven National Laboratory, Upton, New York 11973, USA

10 School of Science and Engineering, The Chinese University of Hong Kong, Shenzhen 518172, China

We report a state-of-the-art lattice QCD calculation of the nucleon gluon parton distribution function employing large-momentum effective theory. The calculation is carried out on the 2+1 flavour CLQCD ensembles with three lattice spacings $a = \{0.105, 0.0897, 0.0775\}$ fm and pion mass of approximately 300 MeV, covering nulceon momenta up to 1.97 GeV. Distillation technique is applied to improve the signal of two-point correlators. We then apply the state-of-the-art hybrid renormalization and one-loop perturbative matching, and extrapolate the result to the continuum and infinite momentum limit. Our result is in agreement with that from global analysis within errors.

Introduction: Parton distribution functions (PDFs) represent fundamental quantities that encode the internal structure of hadrons in terms of their constituent quarks and gluons. Among these, the gluon PDF plays a particularly crucial role in our understanding of quantum chromodynamics (QCD) and has profound implications for high-energy physics phenomenology. The gluon PDF g(x) describes the probability density for finding a gluon carrying a fraction x of the nucleon's momentum, providing essential input for theoretical predictions of hadron-hadron collisions, deep inelastic scattering processes, and precision tests of the Standard Model at hadron colliders.

Despite its fundamental importance, the determination of the gluon PDF has historically presented significant theoretical and computational challenges. Traditional approaches rely on global fits to experimental data from deep inelastic scattering and hadron-hadron collisions [1–6]. However, these phenomenological extractions are inherently model-dependent and face severe limitations in the large-x region where experimental data is sparse and the gluon PDF becomes increasingly uncertain. The lack of direct experimental constraints on the gluon PDF at large x has motivated the development of first-principles theoretical approaches.

The advent of Large Momentum Effective Theory (LaMET) [7–9] has revolutionized the field by enabling first-principle calculations of PDFs from lattice QCD.

LaMET provides a systematic framework for extracting light-cone PDFs from quasi-PDFs, which can be computed directly on the lattice and matched to the physical PDFs through perturbative matching relations. The key insight of LaMET is that when a hadron carries large momentum $P_z \gg \Lambda_{\rm QCD}$, the quasi-PDF approaches the light-cone PDF up to perturbative matching and power corrections that can be systematically controlled. Recent years have witnessed remarkable progress in lattice PDF calculations, with numerous studies successfully extracting quark PDFs for both nucleons and mesons [10–27].

However, lattice calculations of gluon PDFs present unique challenges that have limited their progress compared to quark PDFs. The gluonic operators are notoriously noisy in lattice simulations, requiring sophisticated techniques to extract clean signals. The renormalization of gluonic operators presents additional complications due to mixing with quark operators. Several pioneering studies have made significant progress in gluon PDF calculations, with most employing the pseudo-PDF method [28–36]. The LaMET calculations of the gluon PDF has recently appeared [27, 37, 38], though these studies are performed either at a single lattice spacing without continuum extrapolation or at one finite momentum without infinite momentum extrapolation.

In this paper, we present a comprehensive lattice QCD calculation of the unpolarized gluon PDF of the nu-

Ensemble	$a(\mathrm{fm})$	$L^3 \times T$	$m_{\pi}(\mathrm{MeV})$	$m_{\pi}L$	$N_{\rm conf.}$
C24P29	0.105	$24^3\times72$	292.3(1.0)	3.746(13)	879
E32P29	0.0897	$32^3\times 64$	287.3(2.5)	4.179(36)	900
F32P30	0.0775	$32^3 \times 96$	300.4(1.2)	3.780(15)	777

TABLE I. The simulation setup, including lattice spacing a, lattice size $L^3 \times T$, π mass m_{π} and the number of configurations for each ensemble.

cleon in the framework of LaMET with both continuum limit and infinite momentum extrapolations, which are crucial for obtaining the true light-cone PDF. We perform our calculation on three lattice spacings a = $\{0.0775, 0.0897, 0.105\}$ fm with pion mass of approximately 300 MeV. We use several nucleon momenta up to 1.97GeV to extrapolate to the infinite momentum. The distillation quark smearing method [39] is applied to improve the signal-to-noise ratio of the gluonic matrix elements. We employ the state-of-the-art hybrid renormalization scheme [40] to remove ultraviolet divergences nonperturbatively, and apply one-loop perturbative matching to obtain the light-cone PDF. Our results represent a significant step forward in the precision determination of gluon PDFs from first principles and provide the most complete lattice QCD calculation of the nucleon gluon PDF to date.

Lattice calculations: In this work we use the 2+1 flavor QCD ensembles with tadpole improved tree level Symanzik (TITLS) gauge action and the tadpole improved tree level Clover (TITLC) fermion action generated by CLQCD collaboration [41, 42]. The calculation is performed on three ensembles with three lattice spacings at the similar pion mass around 300 MeV. For each ensemble over 700 configurations are used. The detailed information is given in Table I.

According to LaMET, to obtain light-cone PDF, one starts with calculating bare-matrix elements $\tilde{h}_B(z,P_z,1/a) = \langle P_z|O(z)|P_z\rangle$, which can be extracted from two-point and three-point correlation functions. The gluon operator O(z) adopts the following form which is multiplicatively renormalizable [43, 44]

$$O(z) = M_{tx;tx}(z) + M_{ty;ty}(z) - 2M_{xy;xy}(z),$$
 (1)

with

$$M_{\mu\lambda;\nu\rho}(z) = \sum_{\vec{x}} Tr[F_{\mu\lambda}(\vec{x} + z\hat{z})U(\vec{x} + z\hat{z}, \vec{x})$$
$$F_{\nu\rho}(\vec{x})U(\vec{x}, \vec{x} + z\hat{z})] \tag{2}$$

under fundamental representation. $U(\vec{x}+z\hat{z},\vec{x})$ is the Wilson line introduced to ensure gauge invariance and $F_{\mu\nu}=(\partial_{\mu}A^{a}_{\nu}-\partial_{\nu}A^{a}_{\mu}-gf^{abc}A^{b}_{\mu}A^{c}_{\nu})T^{a}$ is the gauge field tensor. We employ the nucleon interpolating operator $N=P_{+}(u^{T}C\gamma_{5}\gamma_{t}d)u$, where C denotes the charge-conjugation operator and $P^{+}=\frac{1}{2}(1+\gamma_{t})$ is the posi-

tive parity projector. As shown in Ref. [45], this operator has kinematically-enhanced overlap with the ground state at large momentum. The quark propagators are computed for all the time slices using distillation quark smearing method [39]. The number of eigenvectors N_{ev} in the smearing operator is 100 for all the three ensembles. Ten-step hypercubic (HYP) smearing is applied on the gluon operators in order to suppress the linear UV divergence.

The bare matrix elements are then obtained by fitting the ratio of the three-point to two-point correlation functions, the details of the fitting are provided in the supplemental material [46].

Renormalization: The bare matrix elements contain both linear and logarithmic divergences that must be removed via a renormalization procedure. While several nonperturbative renormalization methods have been developed for this purpose [47–52], their renormalization factors can incorporate unwanted nonperturbative effects. To circumvent this issue, we adopt the hybrid scheme [40]. In this approach, the divergences at short distances are removed by dividing the zero-momentum bare matrix element. At long distances, we employ a self-renormalization procedure. The renormalized matrix element is thus defined as:

$$\tilde{h}_{R}(z, P_{z}) = \frac{\tilde{h}_{B}^{n}(z, P_{z}, 1/a)}{\tilde{h}_{B}^{n}(z, P_{z} = 0, 1/a)} \theta(z_{s} - |z|) + \eta_{s} \frac{\tilde{h}_{B}^{n}(z, P_{z}, 1/a)}{Z_{R}(z, 1/a)} \theta(|z| - z_{s}),$$
(3)

where $\tilde{h}_B^n(z,P_z,1/a)$ is the normalized bare matrix element, z_s is introduced to distinguish the short and long distances, and η_s is the scheme conversion factor that ensures the continuity of the renormalized quasi-LF correlation at $z=z_s$. The self-renormalization factor $Z_R(z,1/a)$ takes the following parametrization form, which contains both linear divergence and logarithmic UV divergences:

$$Z_R(z, 1/a, \mu; k, \Lambda_{\text{QCD}}, m_0, d) = \exp\left\{\frac{kz}{a \ln[a\Lambda_{\text{QCD}}]} + m_0 z + \frac{5C_A}{3b_0} \ln\left[\frac{\ln(1/a\Lambda_{\text{QCD}})}{\ln(\mu/\Lambda_{\text{QCD}})}\right] + \frac{1}{2} \ln\left[\left(1 + \frac{d}{\ln[a\Lambda_{\text{QCD}}]}\right)^2\right]\right\},$$
(4)

where the first term is the linear divergence, m_0z denotes a finite-mass contribution from the renormalization ambiguity, and the last two terms come from the resummation of the leading and subleading logarithmic divergences. According to Ref. [13], parameters k is related to the specific discretized action, while d and m_0 are determined by matching to the continuum scheme at short distances. In the $\overline{\rm MS}$ scheme, the short-distance result takes the following form at next-to-leading order

k	1.92(1.18)
$\Lambda_{\rm QCD}({\rm GeV})$	0.59(0.15)
$m_0({ m GeV})$	2.78(1.51)
d	-0.079(0.403)
$\chi^2/\text{d.o.f.}$	0.09

TABLE II. The parameters in the self-renormalization factor determined by fitting the zero-momentum matrix elements to Eq. (6). The $\chi^2/\text{d.o.f.}$ of the fit is also presented.

(NLO):

$$\tilde{h}_{\overline{MS}}^{\text{pert}}(z,\mu) = 1 + \frac{\alpha_s(\mu)C_A}{4\pi} \left(\frac{5}{3} \ln \frac{z^2 \mu^2}{4e^{-2\gamma_E}} + 3\right),$$
 (5)

where γ_E is the Euler-Mascheroni constant. We set the renormalization scale $\mu = 2$ GeV, yielding a running coupling constant $\alpha_s(\mu) = 0.296$.

The parameters in Z_R are determined by fitting the bare matrix elements at zero momentum:

$$\ln \tilde{h}_{B}^{n}(z, P_{z} = 0, 1/a) = \ln[Z_{R}(z, 1/a, \mu; k, \Lambda_{\text{QCD}}, m_{0}, d)] + \begin{cases} \ln[\tilde{h}_{\overline{\text{MS}}}^{\text{pert}}(z, \mu)] & \text{if } z_{0} \leq z \leq z_{1} \\ g(z) - m_{0}z & \text{if } z_{1} < z \end{cases},$$
(6)

where k, $\Lambda_{\rm QCD}$, m_0 , d and g(z) are treated as free parameters. We choose $z_0=0.15$ fm , $z_1=0.3$ fm and the maximum value of z is 1 fm. Note that the value of k here differs from that of the quark quasi-PDF by a factor C_A/C_F at the leading order and then can be significantly larger. The fitting results of the parameters and the corresponding $\chi^2/{\rm d.o.f.}$ are presented in Table II. Although for some parameters the uncertainties appear large, it should be noted that they are strongly correlated and compensate for one another, leading to a reduced uncertainty in the computed self-renormalization factor Z_R .

Fig. 1 illustrates the comparison of the renormalized matrix elements with the perturbative one-loop $\overline{\rm MS}$ results. As shown in the figure, the renormalized matrix elements agree well with the continuum one-loop result at short distance while can deviate from large distance significantly due to non-perturbative IR effects.

The renormalized matrix elements for each ensemble are shown in Fig. 2, with colors denoting different nucleon momenta. All three ensembles show a consistent trend: the matrix elements decay more slowly at higher momenta. For ensemble C24P29 and E32P29, the results converge clearly for $P_z > 1.5$ GeV. For ensemble F32P30 the signal beyond 1.5 GeV is excessively poor and then not shown here. Our future studies will address this limitation by employing momentum smearing techniques to enhance the signal.

The uncertainties of renormalized matrix elements become worse with increasing $\lambda = zP_z$. However, a Fourier

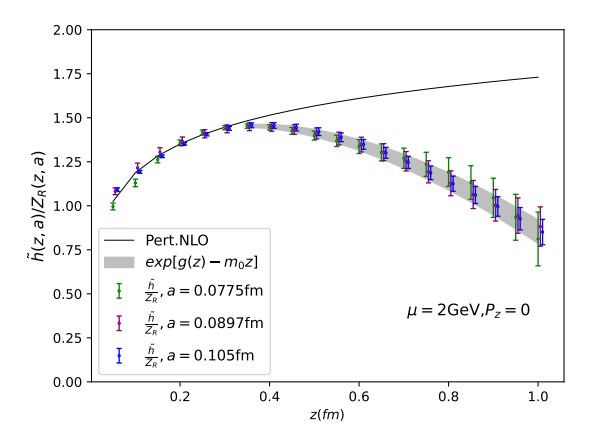


FIG. 1. Comparison of renormalized matrix elements with the perturbative one-loop $\overline{\rm MS}$ results (black curve). Error bars represent the renormalized matrix elements of each lattice spacing. g(z) is the residual from the fitting process and $\exp[g(z)-m_0z]$ (gray band) indicates the a-independent renormalized matrix element.

transform to momentum space requires the quasicorrelator at all distances. To resolve this issue, we follow Ref. [40] and adopt an extrapolation with the following form in the large λ region:

$$\tilde{h}_R(\lambda) = l_1 \lambda^{-a_1} e^{-\lambda/\lambda_0},\tag{7}$$

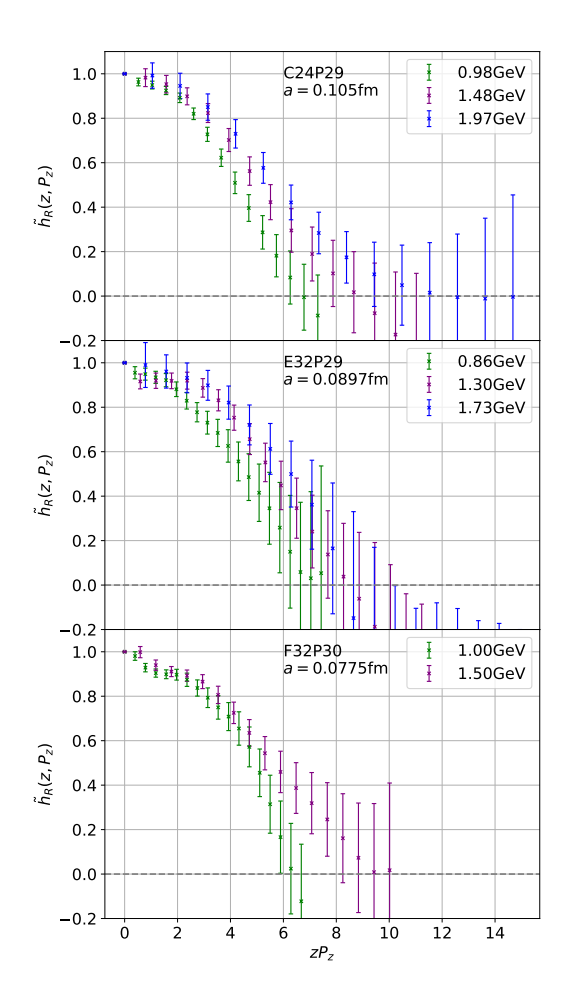
where λ^{-a_1} is associated with a power law behavior of the unpolarized PDFs in the end point region, and the exponential factor accounts for expectation that the correlation length λ_0 of the correlation function is finite at finite momentum [40]. Examples of large λ extrapolation can be found in the supplemental material [46].

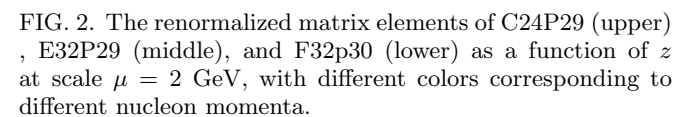
Light-cone PDF: After the λ extrapolation, we can perform a Fourier transform and obtain the x-dependent quasi-PDF in momentum space, then extract the the light-cone PDF through a perturbative matching. The detailed matching formula can be found in the supplemental material [46].

The light-cone PDF obtained after perturbative matching still contains P_z dependence and lattice spacing dependence, which has to be removed by extrapolating to infinite momentum limit and continuum limit:

$$xg(x, P_z, a) = xg_0(x) + a^2 f(x) + a^2 P_z^2 h(x) + \frac{d(x)}{P_z^2},$$
 (8)

where $xg(x, P_z, a)$ represents the PDF obtained on different ensembles and at different momenta and $xg_0(x)$ represents the light-cone PDF extrapolated to continuum limit and infinite-momentum limit. The $a^2f(x)$ term represents the discretization error, the $a^2P_z^2h(x)$ term denotes the momentum-dependent discretization error, and the $d(x)/P_z^2$ term accounts for the leading higher-twist





contribution. Possible higher order correction likes the lattice spacing dependence of d(x) is not statistical significant and then omitted to ensure a stable fit. Additionally, we do not include pion mass dependence in this work, as its effect is expected to be weak based on previous studies [31]. We plan to incorporate finer lattice spacings, multiple pion masses, and higher momenta in future work to improve this extrapolation.

Results of the light-cone PDF $xg(x)/\langle x\rangle$ of three ensembles obtained by perturbative matching are presented in Fig. 3, with $\langle x\rangle=\int_0^1 dx x g(x)$ representing the gluon momentum fraction. The colored bands illustrate the results obtained at different lattice spacings and different momenta. The gray band, repeated across the three figures, illustrates the result extrapolated to infinite momentum limit and continuum limit. Its uncertainty is significantly larger than that before extrapolation. As can be seen for all three ensembles the PDF in the middle-and large-x region is suppressed with the increase of mo-

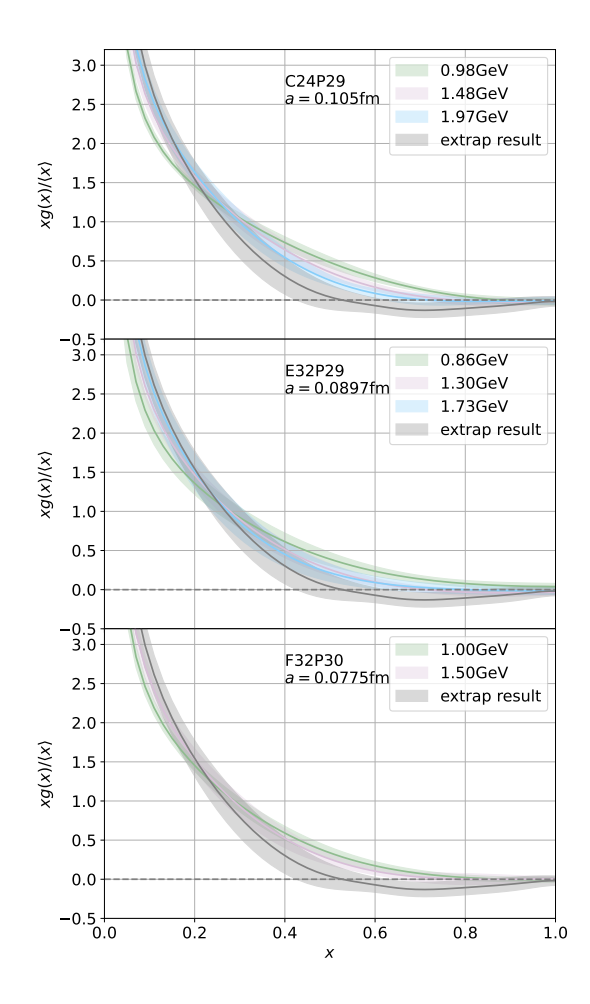


FIG. 3. Results of the light-cone PDF $xg(x)/\langle x \rangle$ of three ensembles. The colored bands illustrate the results obtained at different lattice spacings and different momenta. The gray band, repeated across the three figures, illustrates the result extrapolated to infinite momentum limit and continuum limit. Only statistic uncertainties are considered in the plot.

mentum. After the extrapolation, the value of PDF is consistent with zero with slightly negative central value.

Systematic uncertainties from large- λ extrapolation, perturbative matching, joint continuum and infinite momentum extrapolations, and also choice of z_s are included in this work. The first uncertainty is introduced by the large- λ extrapolation. This error is estimated by choosing different fitting ranges to do the extrapolation. The second is from higher order correction of the perturbative matching, which is estimated by varying the scale from 2 to 4 GeV. The third comes from the extrapolation to continuum and infinite momentum limits, which is estimated by taking the difference between extrapolated result and a=0.0775 fm, $P_z=1.5$ GeV result. The last uncertainty is from the choice of z_s in the hybrid renormalization scheme. We choose $z_s=0.3$ fm, vary it down to $z_s=0.2$ fm and take the difference as

a systematic uncertainty. The detailed analysis of systematic uncertainties can be found in the supplemental material [46].

Our final results for the unpolarized PDF in the continuum and infinite-momentum limit are plotted in Fig. 4. The deep blue band indicates statistical uncertainties of our result, while the light blue band represents the combined effects of both statistical and systematic uncertainties. The gray bands mark the x < 0.2 and x > 0.8regions, where LaMET results are considered unreliable. We compare our results with CT18 NNLO [2], NNPDF NNLO [3] and JAM24 global fit [53], and they are consistent with each other within current uncertainty. We observe that the theoretical and experimental results in the large-x region are both very close to zero, indicating the suppression of the gluon PDF at large x. Our final prediction carries a significantly enlarged uncertainty due to the simultaneous extrapolation to the continuum and infinite-momentum limits. This process, which involves both $1/P_z^2$ and $a^2P_z^2$ terms, demonstrates the non-trivial systematic effects that must be conservatively managed.

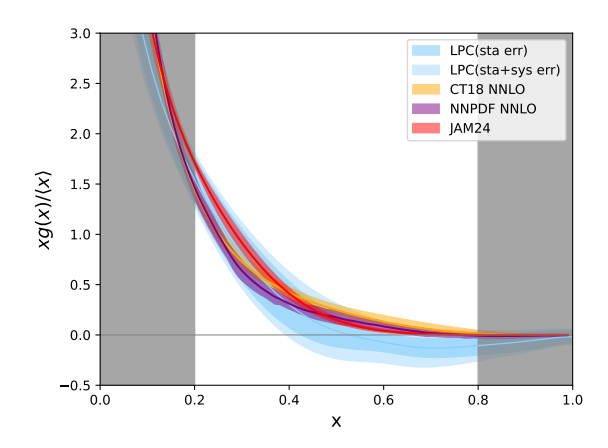


FIG. 4. LPC prediction of unpolarized gluon PDF in the continuum and infinite-momentum limit $xg(x)/\langle x \rangle$ in comparison with global fit results. The deep blue band indicates statistical uncertainties of our result, while the light blue band represents the combined effects of both statistical and systematic uncertainties. The gray bands denote the regions where LaMET results are considered unreliable.

Summary: We have presented a lattice QCD calculation of the gluon PDF of nucleon using the LaMET method. Our calculation was performed on ensembles with three lattice spacings from 0.105 fm to 0.077 fm at a pion mass of approximately 300 MeV. With high statistics, we have used multiple source-sink separations to control the excited-state contamination and applied the state-of-the-art renormalization, matching, and extrapolation procedure. The distillation method was employed to enhance the statistics. We have also studied the momentum and lattice spacing dependence, and extrapolated the result to the infinite-momentum and contin-

uum limit. Our final result is consistent with global fits and another lattice calculation from the MSULat group within the current uncertainties.

Future improvements can be pursued in several directions. The signal quality at large momenta could be enhanced using momentum smearing, while calculations at finer lattice spacings and larger momenta would provide better control over the extrapolations to the infinite momentum and continuum limits. Furthermore, a study of the pion mass dependence would enable a chiral extrapolation. Finally, the renormalization and matching procedures could be refined by implementing renormalization-group resummation [54] and leading-renormalon resummation [55]. Developing these methods may extend the effective range of LaMET and reduce the scale dependence of our final results.

Note added: While this paper was being finalized, Ref. [38] appeared which also computed the unpolarized gluon PDF of the nucleon using a different lattice setup based on gradient flow. In contrast to their calculation, we have performed an extrapolation to the infinite momentum limit, enabling a more direct connection to the unpolarized gluon PDF extracted from global fits. Nevertheless, the results are consistent within errors.

ACKNOWLEDGMENTS

We thank the CLQCD collaboration for providing us with their gauge configurations with dynamical fermions [41, 42], which are generated on HPC cluster of ITP-CAS, IHEP-CAS and CSNS-CAS, the Southern Nuclear Science Computing Center(SNSC), the Sivuan-1 cluster supported by the Center for High-Performance Computing at Shanghai Jiao Tong University, and the Dongjiang Yuan Intelligent Computing Center. We are grateful to Yushan Su for the valuable discussion and comments. The numerical calculations in this paper were carried out at the Dongjiang Yuan Intelligent Computing Center, the HPC cluster of ITP-CAS and the Southern Nuclear Science Computing Center(SNSC). This work is supported in part by National Natural Science Foundation of China (NSFC) under Grant No. 12293060, No. 12375080, No. 12293061, No. 12293062, No. 12175279, 12525504, No. 12293065, No. 12047503, No. 12435002, No. 12375080, No. 11975051 and 12447101, the Strategic Priority Research Program of the Chinese Academy of Sciences with Grant No. XDB34030301, No. XDB34030303 and No. YSBR-101, the Guangdong Major Project of Basic and Applied Basic Research No. 2020B0301030008, the Education Integration Young Faculty Project of University of Chinese Academy of Sciences, the Ministry of Science and Technology of China under Grant No. 2024YFA1611004, CUHK-Shenzhen under grant No. UDF01002851, and a NSFC-DFG joint grant under Grant No. 12061131006 and SCHA 458/22

and the GHfund A No. 202107011598.

- * Corresponding author: liuming@impcas.ac.cn
- † Corresponding author: pengsun@impcas.ac.cn
- [‡] Corresponding author: ybyang@itp.ac.cn
- § Corresponding author: zhangjianhui@cuhk.edu.cn
- S. Bailey, T. Cridge, L. A. Harland-Lang, A. D. Martin, and R. S. Thorne, Eur. Phys. J. C 81, 341 (2021), 2012.04684.
- [2] T.-J. Hou et al., Phys. Rev. D 103, 014013 (2021), 1912.10053.
- [3] R. D. Ball et al. (NNPDF), Eur. Phys. J. C 77, 663 (2017), 1706.00428.
- [4] R. D. Ball et al. (NNPDF), Eur. Phys. J. C 82, 428 (2022), 2109.02653.
- [5] A. Accardi, L. T. Brady, W. Melnitchouk, J. F. Owens, and N. Sato, Phys. Rev. D 93, 114017 (2016), 1602.03154.
- [6] S. Dulat, T.-J. Hou, J. Gao, M. Guzzi, J. Huston, P. Nadolsky, J. Pumplin, C. Schmidt, D. Stump, and C. P. Yuan, Phys. Rev. D 93, 033006 (2016), 1506.07443.
- [7] X. Ji, Phys. Rev. Lett. **110**, 262002 (2013), 1305.1539.
- [8] X. Ji, Sci. China Phys. Mech. Astron. 57, 1407 (2014), 1404.6680.
- [9] X. Ji, J.-H. Zhang, and Y. Zhao, Nucl. Phys. B 924, 366 (2017), 1706.07416.
- [10] H.-W. Lin, J.-W. Chen, X. Ji, L. Jin, R. Li, Y.-S. Liu, Y.-B. Yang, J.-H. Zhang, and Y. Zhao, Phys. Rev. Lett. 121, 242003 (2018), 1807.07431.
- [11] Y.-S. Liu et al. (Lattice Parton), Phys. Rev. D 101, 034020 (2020), 1807.06566.
- [12] Q.-A. Zhang et al. (Lattice Parton), Phys. Rev. Lett. 125, 192001 (2020), 2005.14572.
- [13] Y.-K. Huo et al. (Lattice Parton (LPC)), Nucl. Phys. B 969, 115443 (2021), 2103.02965.
- [14] J. Hua, M.-H. Chu, P. Sun, W. Wang, J. Xu, Y.-B. Yang, J.-H. Zhang, and Q.-A. Zhang (Lattice Parton), Phys. Rev. Lett. 127, 062002 (2021), 2011.09788.
- [15] M.-H. Chu et al. (Lattice Parton (LPC)), Phys. Rev. D 106, 034509 (2022), 2204.00200.
- [16] K. Zhang, X. Ji, Y.-B. Yang, F. Yao, and J.-H. Zhang (Lattice Parton (LPC)), Phys. Rev. Lett. 129, 082002 (2022), 2205.13402.
- [17] J. Hua et al. (Lattice Parton), Phys. Rev. Lett. 129, 132001 (2022), 2201.09173.
- [18] M.-H. Chu et al. (Lattice Parton (LPC)), JHEP 08, 172 (2023), 2306.06488.
- [19] F. Yao et al. (Lattice Parton), Phys. Rev. Lett. 131, 261901 (2023), 2208.08008.
- [20] J.-C. He, M.-H. Chu, J. Hua, X. Ji, A. Schäfer, Y. Su, W. Wang, Y.-B. Yang, J.-H. Zhang, and Q.-A. Zhang (Lattice Parton Collaboration (LPC)), Phys. Rev. D 109, 114513 (2024), 2211.02340.
- [21] M.-H. Chu et al. (Lattice Parton), Phys. Rev. D 109, L091503 (2024), 2302.09961.
- [22] K. Zhang, Y.-K. Huo, X. Ji, A. Schaefer, C.-J. Shi, P. Sun, W. Wang, Y.-B. Yang, and J.-H. Zhang (Lattice Parton), Phys. Rev. D 110, 074505 (2024), 2405.14097.
- [23] C. Chen, Y. Geng, L. Liu, P. Sun, Y.-B. Yang, F. Yao, J.-H. Zhang, and K. Zhang (CLQCD, Lattice Parton),

- Phys. Rev. D 111, 074506 (2025), 2408.12819.
- [24] X.-Y. Han et al. (Lattice Parton), Phys. Rev. D 111, 034503 (2025), 2410.18654.
- [25] L. Ma et al. (LPC) (2025), 2502.11807.
- [26] Q.-A. Zhang, J.-C. He, M.-H. Chu, J. Hua, X. Ji, A. Schäfer, Y. Su, W. Wang, Y.-B. Yang, and J.-H. Zhang, PoS QNP2024, 052 (2025).
- [27] W. Good, K. Hasan, and H.-W. Lin, J. Phys. G 52, 035105 (2025), 2409.02750.
- [28] Z.-Y. Fan, Y.-B. Yang, A. Anthony, H.-W. Lin, and K.-F. Liu, Phys. Rev. Lett. 121, 242001 (2018), 1808.02077.
- [29] Z. Fan, R. Zhang, and H.-W. Lin, Int. J. Mod. Phys. A 36, 2150080 (2021), 2007.16113.
- [30] T. Khan et al. (HadStruc), Phys. Rev. D 104, 094516 (2021), 2107.08960.
- [31] Z. Fan, W. Good, and H.-W. Lin, Phys. Rev. D **108**, 014508 (2023), 2210.09985.
- [32] W. Good, Z. Fan, and H.-W. Lin, in 30th International Workshop on Deep-Inelastic Scattering and Related Subjects (2023), 2307.06916.
- [33] J. Delmar, C. Alexandrou, K. Cichy, M. Constantinou, and K. Hadjiyiannakou, Phys. Rev. D 108, 094515 (2023), 2310.01389.
- [34] Z. Fan and H.-W. Lin, Phys. Lett. B 823, 136778 (2021), 2104.06372.
- [35] W. Good, K. Hasan, A. Chevis, and H.-W. Lin, Phys. Rev. D 109, 114509 (2024), 2310.12034.
- [36] A. Salas-Chavira, Z. Fan, and H.-W. Lin, Phys. Rev. D 106, 094510 (2022), 2112.03124.
- [37] W. Good, F. Yao, and H.-W. Lin (2025), 2505.13321.
- [38] A. NieMiera, W. Good, H.-W. Lin, and F. Yao (2025), 2510.17758.
- [39] M. Peardon, J. Bulava, J. Foley, C. Morningstar, J. Dudek, R. G. Edwards, B. Joo, H.-W. Lin, D. G. Richards, and K. J. Juge (Hadron Spectrum), Phys. Rev. D 80, 054506 (2009), 0905.2160.
- [40] X. Ji, Y. Liu, A. Schäfer, W. Wang, Y.-B. Yang, J.-H. Zhang, and Y. Zhao, Nucl. Phys. B 964, 115311 (2021), 2008.03886.
- [41] Z.-C. Hu et al. (CLQCD), Phys. Rev. D 109, 054507 (2024), 2310.00814.
- [42] H.-Y. Du et al. (CLQCD), Phys. Rev. D 111, 054504 (2025), 2408.03548.
- [43] J.-H. Zhang, X. Ji, A. Schäfer, W. Wang, and S. Zhao, Phys. Rev. Lett. 122, 142001 (2019), 1808.10824.
- [44] I. Balitsky, W. Morris, and A. Radyushkin, Phys. Lett. B 808, 135621 (2020), 1910.13963.
- [45] R. Zhang, A. V. Grebe, D. C. Hackett, M. L. Wagman, and Y. Zhao (2025), 2501.00729.
- [46] See the supplemental material for further details on the theoretical framework and data analysis. (2025).
- [47] J.-W. Chen, X. Ji, and J.-H. Zhang, Nucl. Phys. B 915, 1 (2017), 1609.08102.
- [48] T. Izubuchi, X. Ji, L. Jin, I. W. Stewart, and Y. Zhao, Phys. Rev. D 98, 056004 (2018), 1801.03917.
- [49] C. Alexandrou, K. Cichy, M. Constantinou, K. Hadjiyiannakou, K. Jansen, H. Panagopoulos, and F. Steffens, Nucl. Phys. B 923, 394 (2017), 1706.00265.
- [50] A. Radyushkin, Phys. Rev. D 98, 014019 (2018), 1801.02427.
- [51] V. M. Braun, A. Vladimirov, and J.-H. Zhang, Phys. Rev. D 99, 014013 (2019), 1810.00048.
- [52] Z.-Y. Li, Y.-Q. Ma, and J.-W. Qiu, Phys. Rev. Lett. 122, 062002 (2019), 1809.01836.

- [53] T. Anderson, W. Melnitchouk, and N. Sato (2024), 2501.00665.
- [54] R. Zhang, J. Holligan, X. Ji, and Y. Su, Phys. Lett. B 844, 138081 (2023), 2305.05212.
- [55] Y. Su, J. Holligan, X. Ji, F. Yao, J.-H. Zhang, and R. Zhang, Nucl. Phys. B 991, 116201 (2023), 2209.01236.
- [56] I. Balitsky, W. Morris, and A. Radyushkin, Phys. Rev. D 105, 014008 (2022), 2111.06797.
- [57] F. Yao, Y. Ji, and J.-H. Zhang, JHEP 11, 021 (2023), 2212.14415.

SUPPLEMENTAL MATERIAL

Theoretical framework

The light-cone PDF of gluon under adjoint representation is defined as

$$xg(x,\mu) = \int \frac{dz^{-}}{2\pi P^{+}} e^{-ixP^{+}z^{-}} \times \langle P|F^{a}_{+\mu}(z^{-})U^{ab}(z^{-},0)F^{b\mu}_{+\mu}(0)(\mu)|P\rangle, \quad (9)$$

where $z^{\pm} = \frac{1}{2}(z^0 \pm z^3)$ is the space time coordinate along lightcone direction. The Wilson line along the light-cone direction

$$U(z^{-},0) = \mathcal{P} \exp\left[ig \int_{0}^{z^{-}} d\eta^{-} A^{+}(\eta^{-})\right]$$
 (10)

is introduced to ensure gauge invariance of the non-local bilinear operator , with $A_{\mu}^{bc}=if^{abc}A_{\mu}^{a}$ representing the gauge field under adjoint representation.

According to LaMET, the light-cone PDF $yg(y,\mu)$ can be extracted from the quasi-PDF $x\tilde{g}(x,P_z)$ through a matching formula:

$$x\tilde{g}(x, P_z) = \int_{-\infty}^{\infty} \frac{dy}{|y|} C_{\text{hybrid}} \left(\frac{x}{y}, \lambda_s, \frac{\mu}{y P_z}\right) y g(y, \mu) + \mathcal{O}\left(\frac{\Lambda_{\text{QCD}}^2}{(x P_z)^2}, \frac{\Lambda_{\text{QCD}}^2}{((1 - x) P_z)^2}\right), (11)$$

where $C_{\text{hybrid}}\left(\frac{x}{y}, \lambda_s, \frac{\mu}{yP_z}\right)$ represents the perturbative matching kernel in momentum space. Refs. [44, 56] provide the coordinate-space perturbative matching kernel up to next-to-leading order (NLO) in the ratio scheme. We subsequently derive the momentum-space counterpart through a direct Fourier transform, implementing the methodology detailed in Ref. [57]. The corresponding perturbative kernel up to NLO in the hybrid and ratio scheme reads

$$C_{\text{ratio}}\left(\xi, \frac{\mu}{yP_z}\right) = \delta\left(1 - \xi\right) + \frac{\alpha_s(\mu)C_A}{2\pi} \begin{cases} \left[\frac{2(1 - \xi + \xi^2)^2}{1 - \xi} \ln \frac{\xi}{\xi - 1} + \frac{11 - 28\xi + 18\xi^2 - 12\xi^3}{6(1 - \xi)}\right]_+ & \xi > 1\\ \left[\frac{2(1 - \xi + \xi^2)^2}{1 - \xi} \left(-\ln \frac{\mu^2}{4y^2 P_z^2} + \ln(\xi(1 - \xi))\right) - \frac{15 - 56\xi + 102\xi^2 - 96\xi^3 + 48\xi^4}{6(1 - \xi)}\right]_+ & 0 < \xi < 1\\ \left[\frac{-2(1 - \xi + \xi^2)^2}{1 - \xi} \ln \frac{\xi}{\xi - 1} - \frac{11 - 28\xi + 18\xi^2 - 12\xi^3}{6(1 - \xi)}\right]_+ & \xi < 0, \end{cases}$$

$$(12)$$

$$C_{\text{hybrid}}(\xi, \lambda_s, \frac{\mu}{yP_z}) = C_{\text{ratio}}\left(\xi, \frac{\mu}{yP_z}\right) + \frac{\alpha_s(\mu)C_A}{2\pi} \frac{5}{6} \left(-\frac{1}{|1-\xi|} + \frac{2\text{Si}((1-\xi)|y|\lambda_s)}{\pi(1-\xi)}\right)_+,\tag{13}$$

with $\xi = \frac{x}{u}$.

The quasi PDF, which can be directly calculated on lattice, is defined as:

$$x\tilde{g}(x, P_z) = \frac{1}{N} \int \frac{dz}{2\pi P_z} e^{-ixzP_z} \tilde{h}_R(z, P_z), \qquad (14)$$

where $\tilde{h}_R(z, P_z) = \langle P|O(z)|P\rangle_R$ is the renormalized matrix element with O(z) representing a linear combination of gluon operator $M_{\mu\lambda,\nu\rho}(z)$, as shown in Eq. 1 and $N = \frac{(P_z)^2}{(P_t)^2}$ is the normalization factor. The expression of $M_{\mu\lambda,\nu\rho}(z)$ under adjoint representation is

$$M_{\mu\lambda,\nu\rho}(z) = F^a_{\mu\lambda}(z)U^{ab}(z,0)F^b_{\nu\rho}(0).$$
 (15)

On lattice the calculation is performed under fundamental representation where the expression of $M_{\mu\lambda,\nu\rho}(z)$ is changed into Eq. 2.

Bare matrix element

Two-point and three-point correlators

Bare matrix elements $\tilde{h}_B(z, P_z)$ can be obtained by calculating two-point and three-point correlators. Nucleon's two-point correlator (2pt) is defined as

$$C_{2\text{pt}}(P_z; t_{\text{sep}}) = \sum_{t_0} \langle 0|N(P_z; t_0 + t_{\text{sep}})N^{\dagger}(P_z; t_0)|0\rangle$$
(16)

with

$$N(\vec{P};t) = \sum_{\vec{x}} e^{-i\vec{x}\cdot\vec{P}} P_{+}(u^{T}C\gamma_{5}\gamma_{t}d)u(\vec{x};t)$$
 (17)

representing the nucleon operator [45]. The three-point

correlator (3pt) is defined as

$$C_{3\text{pt}}(P_z; z; t_{\text{sep}}, t)$$

= $\sum_{t_0} \langle 0|N(P_z; t_0 + t_{\text{sep}})O(z; t_0 + t)N^{\dagger}(P_z; t_0)|0\rangle$. (18)

On lattice the three-point correlator can be obtained by calculating the disconnected insertion as shown in Fig 5. It can be represented as:

$$C_{3\text{pt}}(P_z; z; t_{\text{sep}}, t) = \sum_{t_0} (O(z; t_0 + t) - \langle O(z; t_0 + t) \rangle) \times (C_{2\text{pt}}(P_z; t_0 + t_{\text{sep}}, t_0) - \langle C_{2\text{pt}}(P_z; t_0 + t_{\text{sep}}, t_0) \rangle).$$
(19)

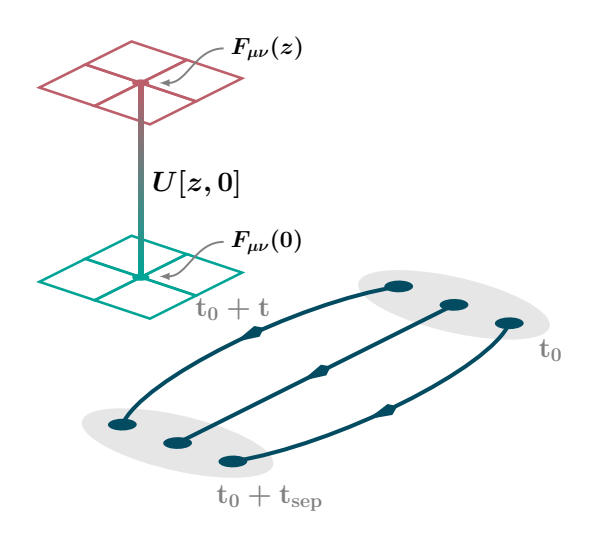


FIG. 5. Illustration of the three-point correlator of gluon.

Fitting for bare matrix elements

Considering the dominated contribution of ground state and first excited state, the two-point correlator $C_{2\mathrm{pt}}(P_z;t_{\mathrm{sep}})$ and three-point correlator $C_{3\mathrm{pt}}(P_z;z;t,t_{\mathrm{sep}})$ can be decomposed as

$$C_{\text{2pt}}(P_z; t_{\text{sep}}) = |\mathcal{A}_0|^2 e^{-E_0 t_{\text{sep}}} + |\mathcal{A}_1|^2 e^{-E_1 t_{\text{sep}}},$$

$$C_{\text{3pt}}(P_z; z; t, t_{\text{sep}}) = |\mathcal{A}_0|^2 \langle 0|O(z; t)|0\rangle e^{-E_0 t_{\text{sep}}}$$

$$+ |\mathcal{A}_1|^2 \langle 1|O(z; t)|1\rangle e^{-E_1 t_{\text{sep}}}$$

$$+ \mathcal{A}_1 \mathcal{A}_0^* \langle 1|O(z; t)|0\rangle e^{-E_1 (t_{\text{sep}} - t)} e^{-E_0 t}$$

$$+ \mathcal{A}_0 \mathcal{A}_1^* \langle 0|O(z; t)|1\rangle e^{-E_0 (t_{\text{sep}} - t)} e^{-E_1 t},$$
(20)

where $\langle 0|O(z;t)|0\rangle$ is the desired ground-state quasimatrix element, $|n\rangle$ represents the *n*th excited state, $\mathcal{A}_{0,1}$ are amplitudes depending on smearing parameters, $E_{0,1}$ are the ground-state and excited-state energy, respectively.

Ensemble	$P_z(\mathrm{GeV})$	$t_{\rm sep}/a$	$n_{\rm ex}$
C24P29	0	[7, 18]	3
	0.98	[7,14]	3
	1.48	[7,11]	3
	1.97	[6,10]	2
E32P29	0	[8, 16]	3
	0.86	[8, 16]	3
	1.3	[8, 14]	3
	1.73	[8, 12]	3
F32P30	0	[9, 16]	3
	1.00	[9, 16]	3
	1.50	[9, 14]	3

TABLE III. Information on the nucleon's momentum P_z , the t_{sep} used for fitting, and n_{ex} , the number points excluded for both sides of each t_{sep} .

The ratio of three-to-two-point correlator can thus be decomposed into the following fitting form

$$R_{3\text{pt}}(P_z; t_{\text{sep}}, t) = \frac{C_{3\text{pt}}(P_z; t_{\text{sep}}, t)}{C_{2\text{pt}}(P_z; t_{\text{sep}})}$$

$$\approx c_0 + c_1 e^{-\Delta E(t_{\text{sep}} - t)} + c_1 e^{-\Delta E t} + c_2 e^{-\Delta E t_{\text{sep}}}, \quad (21)$$

where c_0 corresponds to the bare quasimatrix element and $\Delta E = E_1 - E_0$ denotes the energy gap between the ground state and the first excited state. The terms $c_1 e^{-\Delta E(t_{\text{sep}}-t)} + c_1 e^{-\Delta E t}$, often referred to as the transition terms, dominate over the scattering term $c_2 e^{-\Delta E t_{\text{sep}}}$ at large t_{sep} . In this way we can further ignore the scattering term and simplify the finalized fitting form into

$$R_{3\text{pt}}(P_z; t_{\text{sep}}, t) \approx c_0 + c_1 e^{-\Delta E(t_{\text{sep}} - t)} + c_1 e^{-\Delta E t}$$
. (22)

The ratio is taken after calculating 3000 bootstrap resamples of the three-point and two-point correlator. We perform a joint-fitting incorporating both $z=n_za$ and z=0 data to have a better constraint on ΔE . For each $t_{\rm sep}$ we exclude the $n_{\rm ex}$ points near source and sink to reduce contamination from higher excited states.

In Fig. 9 we compare the fitting result using different fitting range by altering $n_{\rm ex}$ and the minimum $t_{\rm sep}$. The $n_{\rm ex}=2$ fitting results are inconsistent with $n_{\rm ex}=3$ results , indicating that there are still unignorable higher excited state contamination when $n_{\rm ex}=2$. The fitting result doesn't change when $t_{\rm sep}^{min}\geq 7a$ and $n_{\rm ex}\geq 3$. In this way we take $t_{\rm sep}^{min}=7a$, $n_{\rm ex}=3$ as the most reasonable fitting range, which yield the smallest uncertainty while fully excluding higher excited-state contamination. For other momenta and ensembles, the fitting ranges are also settled the same way.

The optimal fitting range of different momenta are shown in table III. In Fig. 10 we plot the bare matrix elements obtained by using the optimal fitting range.

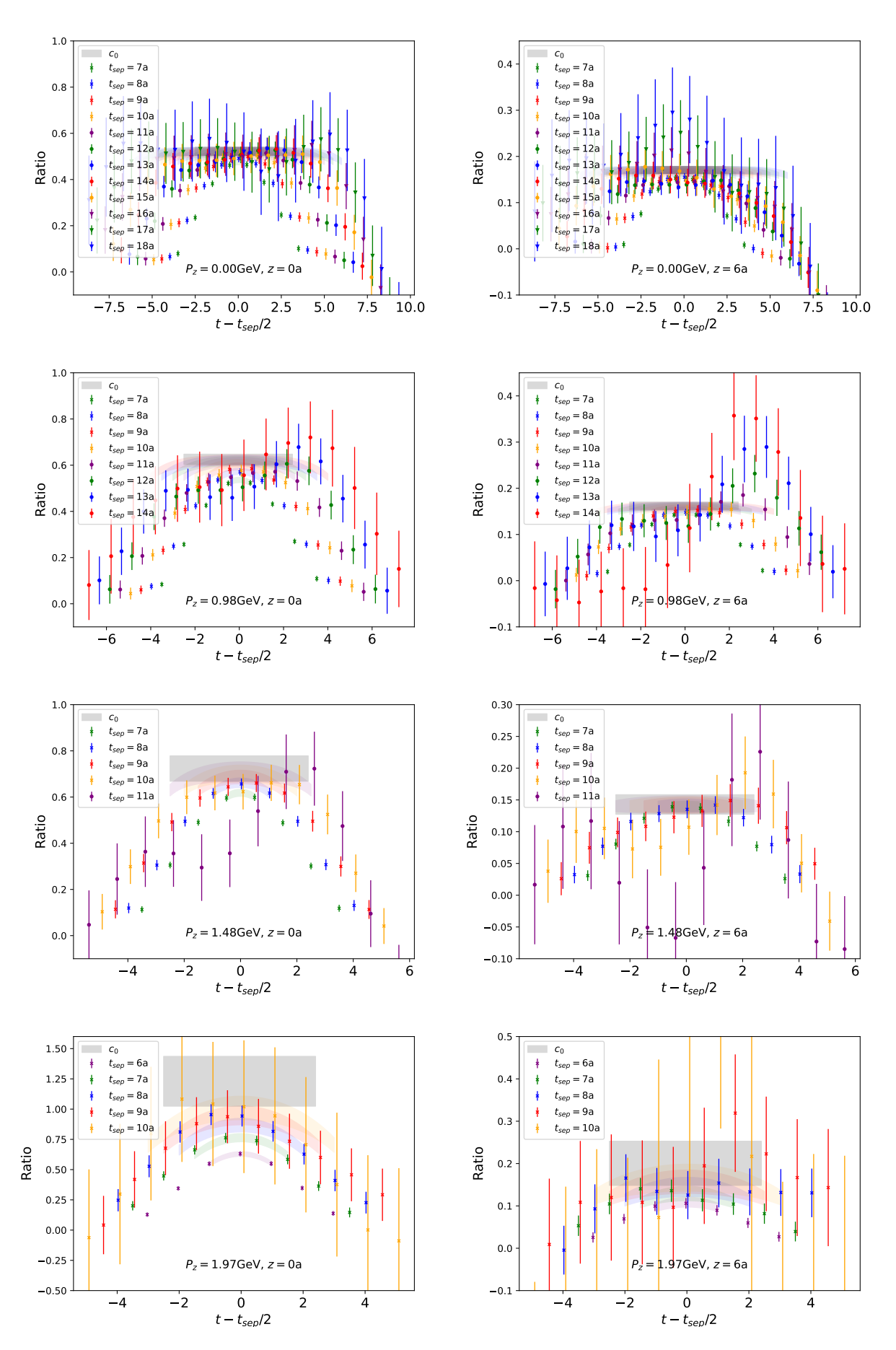


FIG. 6. The ratio of three-to-two point correlator and the fitting results for bare matrix elements of ensemble C24P29 under different momenta. We compare the lattice data of the ratio (error bars) and results predicted by the fitting (colored bands). The ground-state contribution c_0 obtained by the fitting is shown as the gray band.

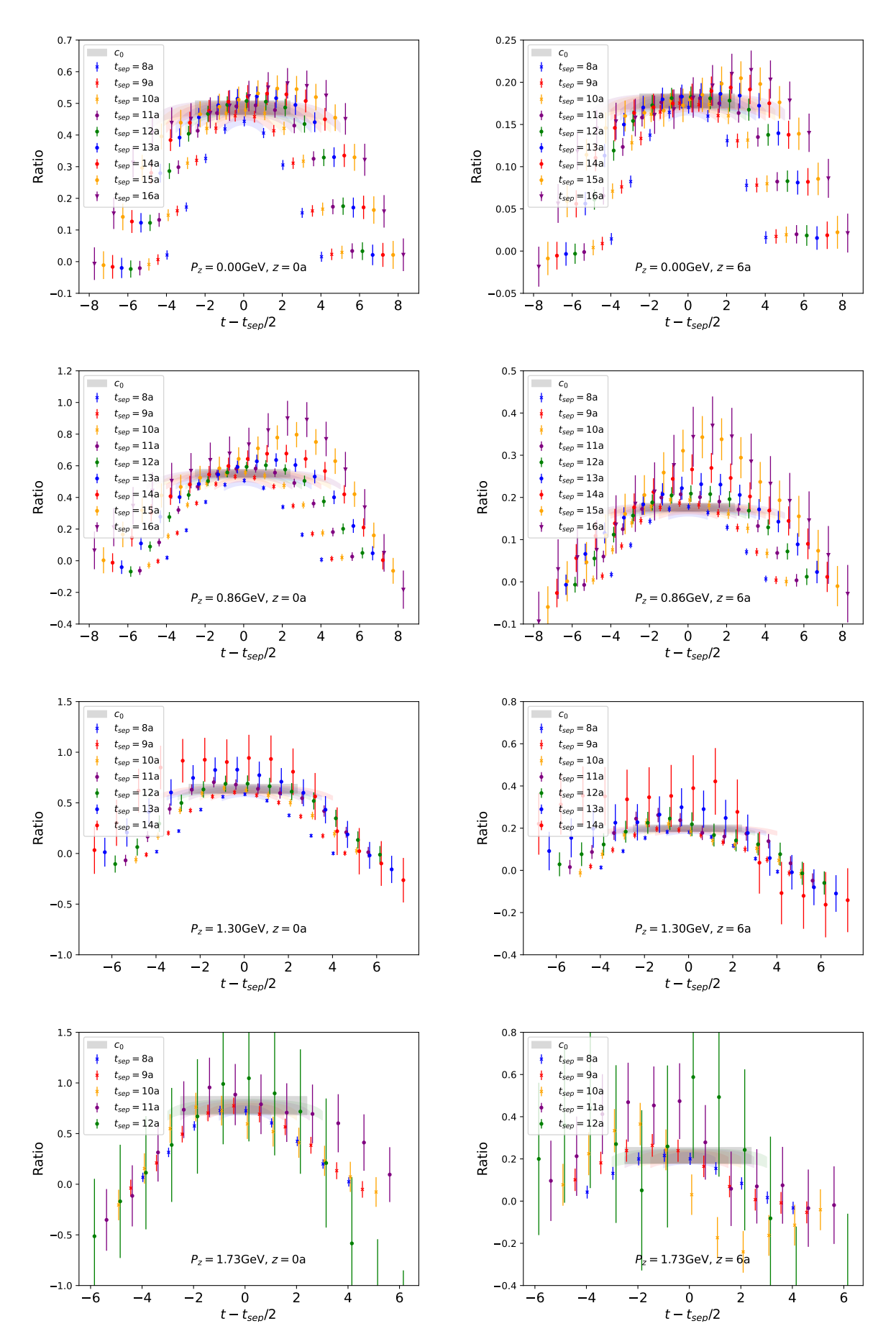


FIG. 7. The ratio of three-to-two point correlator and the fitting results for bare matrix elements of ensemble E32P29 under different momenta. We compare the lattice data of the ratio (error bars) and results predicted by the fitting (colored bands). The ground-state contribution c_0 obtained by the fitting is shown as the gray band.

Ensemble	P_z	default range	new range
	(GeV)	(aP_z)	(aP_z)
C24P29	0.98	[10, 14]	[8, 14]
	1.48	[7, 11]	[5, 11]
	1.97	[6, 10]	[4, 10]
E32P29	0.86	[12, 16]	[10, 16]
	1.3	[9, 13]	[7, 13]
	1.73	[7, 11]	[5, 11]
F32P30	1.00	[10, 15]	[8, 15]
	1.50	[8, 15]	[7, 15]
-			

TABLE IV. The default fitting range and new fitting range for λ extrapolation. The systematic uncertainties brought by λ extrapolation is estimated by taking the difference between results obtained at default extrapolation range and new extrapolation range.

Large- λ extrapolation

Performing the Fourier transform to momentum space requires the renormalized matrix elements across the entire coordinate space. A direct truncation would introduce oscillation into the momentum-space results. This issue can be resloved by performing extrapolation using Eq. 7 to complete the results in the large- λ region. In Fig. 11, we show the extrapolation of the renormalized matrix elements of ensemble C24P29 under different momenta. As can be seen from the plot the extrapolation results agree well with lattice data in fit range and we replace the lattice data with extrapolated results starting from the end of the fitting range.

Estimation of systematic and statistic uncertainties

The systematic uncertainties of our final result arise from four primary sources:

 λ extrapolation: We take the difference between the results from two fitting ranges shown in Table IV as the systematic uncertainty brought by λ extrapolation.

Renormalization scale dependence: In our default case the renormalization scale μ is taken as 2 GeV, with $\alpha_s(\mu) = 0.296$. To explore the systematic brought by renormalization scale, we vary μ to 4 GeV and $\alpha_s(\mu)$ to 0.23. We include the difference of their central values in the systematic uncertainties.

Infinite momentum and continuum-limit extrapolation: To account for the systematic uncertainty due to combined extrapolation in Eq. 8, we take the difference between the combined extrapolation result and the result at smallest lattice spacing a=0.0775 fm and momentum $P_z=1.5$ GeV as an estimate.

Hybrid scheme z_s choice: The systematic bias brought by the choice of z_s is obtained by taking the difference between the results at $z_s=0.3$ fm (default case) and $z_s=0.2$ fm.

In Fig. 12 we show the central value of the gluon PDF and all the uncertainties. These uncertainties are added in quadrature and the square root is taken to obtain the full uncertainty.

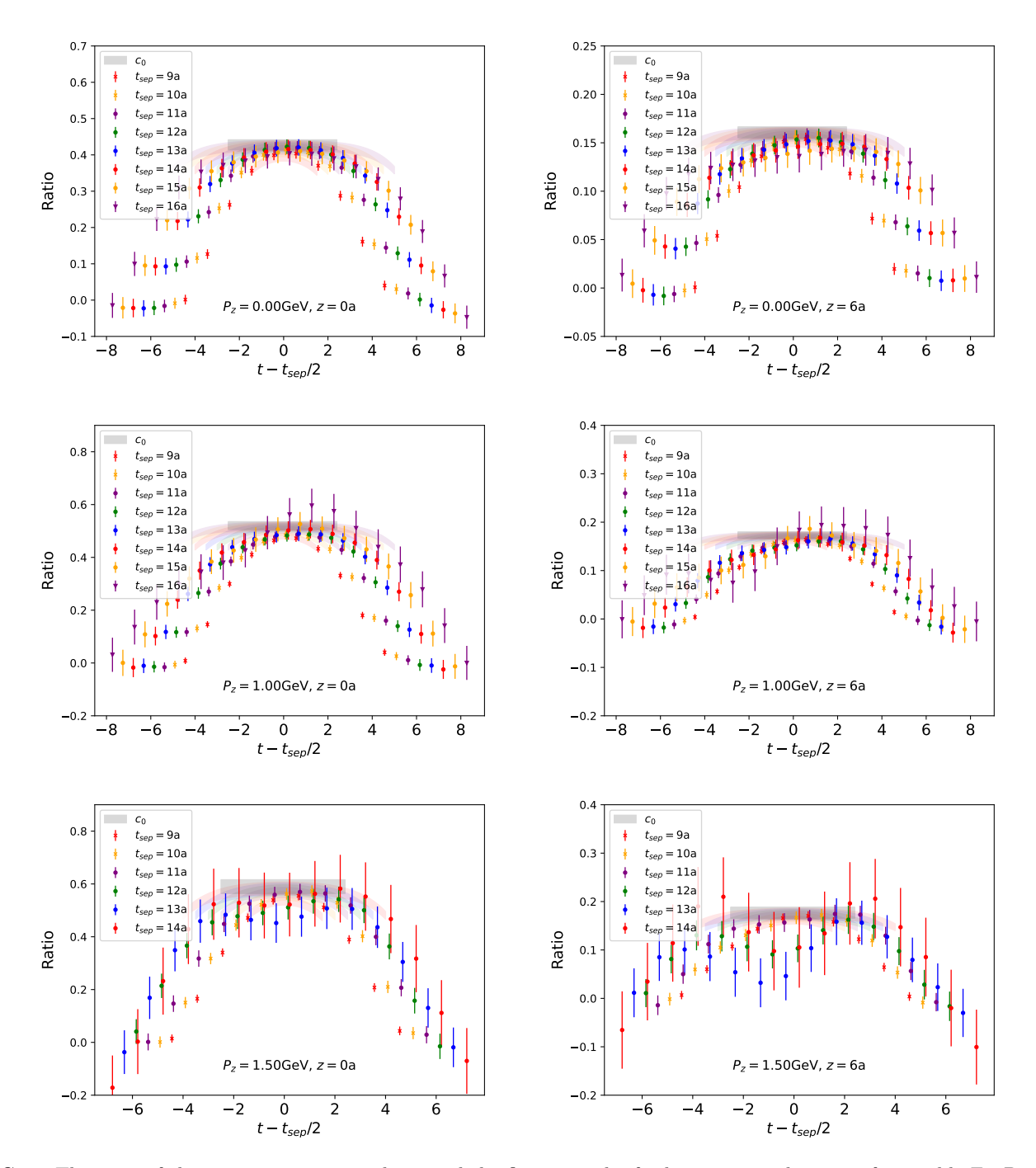


FIG. 8. The ratio of three-to-two point correlator and the fitting results for bare matrix elements of ensemble F32P30 under different momenta. We compare the lattice data of the ratio (error bars) and results predicted by the fitting (colored bands). The ground-state contribution c_0 obtained by the fitting is shown as the gray band.

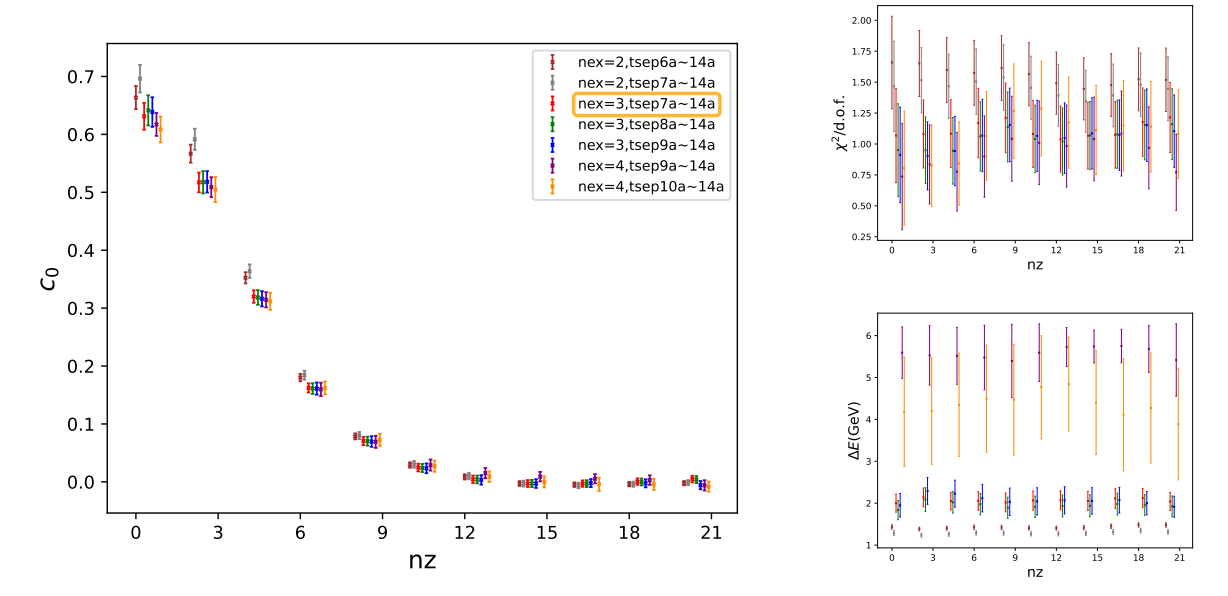
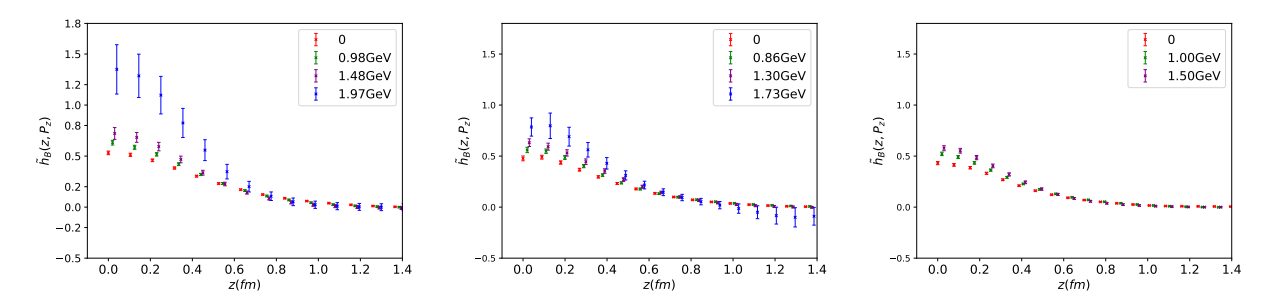


FIG. 9. The fitting result of c_0 , ΔE , and $\chi^2/\text{d.o.f.}$ as a function of z, taking the $P_z = 0.98$ GeV case of ensemble C24P29 as an example. The result using different range is represented using different colors.



 $FIG.\ 10.\ Bare\ matrix\ elements\ of\ C24P29\ (left)\ ,\ E32P29\ (middle),\ and\ F32P30(right)\ obtained\ by\ fitting\ the\ ratio\ of\ three-to-two-point\ correlators.$ The results of different momenta are represented by different colors.

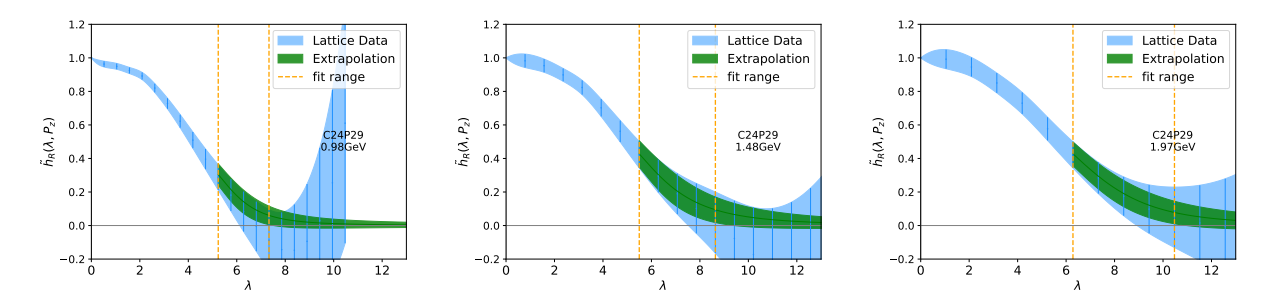


FIG. 11. The large- λ extrapolation of renormalized matrix elements for ensemble C24P29. The blue band and green band represents lattice data and extrapolated results respectively and the fit range for Eq. 7 is marked by orange dashed lines.

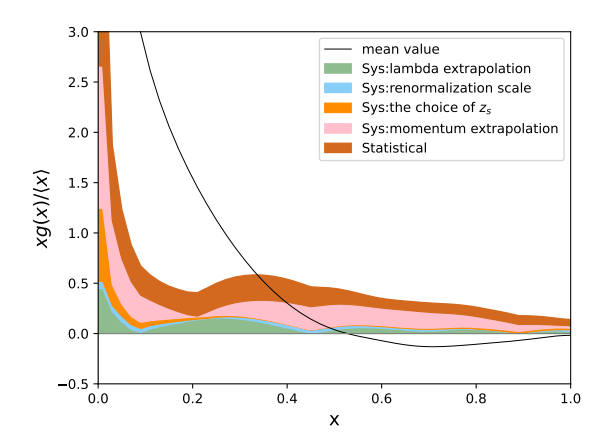


FIG. 12. Estimation of statistical and systematic uncertainties. The width of the (nonoverlapping) colored bands denotes the size of each uncertainty (these uncertainties are added in quadrature and the square root is taken to obtain the full uncertainty). The black curve is the mean value obtained at $z_s=0.3$ fm, $\mu=2$ GeV, the default lambda extrapolation range shown in Table IV and extrapolated to continuum and infinite momentum limit.